Title

Cell derived matrices from bovine corneal endothelial cells as a model to study cellular dysfunction

Authors

Jalilian, Iman

Muppala, Santoshi

Ali, Maryam

et al.

Publication Date

2023

DOI

10.1016/j.exer.2022.109303

Peer reviewed

HHS Public Access

Author manuscript

Exp Eye Res. Author manuscript; available in PMC 2024 August 27.

Published in final edited form as:

Exp Eye Res. 2023 January ; 226: 109303. doi:10.1016/j.exer.2022.109303.

Cell derived matrices from bovine corneal endothelial cells as a model to study cellular dysfunction

Iman Jalilian[a], **Santoshi Muppala**[a,b], **Maryam Ali**[a], **Johnathon D Anderson**[e], **Brett Phinney**[f], **Michelle Salemi**[f], **Phillip A. Wilmarth**[g], **Christopher J Murphy**[a,h], **Sara M Thomasy**[a,h,*], **VijayKrishna Raghunathan**[c,d,*]

[a]Department of Surgical and Radiological Sciences, School of Veterinary Medicine, University of California, Davis, CA, 95616, USA

[b]Cleveland Clinic, Cleveland, OH, 44195, USA

[c]Department of Basic Sciences, College of Optometry

[d]Department of Biomedical Engineering, Cullen College of Engineering, University of Houston, Houston, TX, 77204, USA

[e]Department of Otolaryngology, School of Medicine, University of California, Davis, Sacramento, CA, 95817, USA

[f]Proteomics Core, University of California, Davis Genome Center, Davis, CA, 95616, USA

[g]Proteomics Shared Resources, Oregon Health and Science University, Portland, OR, 97239, USA

[h]Department of Ophthalmology & Vision Science, School of Medicine, UC Davis Medical Center, Sacramento, CA, 95817, USA

Abstract

Purpose: Fuchs endothelial corneal dystrophy (FECD) is a progressive corneal disease that impacts the structure and stiffness of the Descemet's membrane (DM), the substratum for corneal endothelial cells (CECs). These structural alterations of the DM could contribute to the loss of the CECs resulting in corneal edema and blindness. Oxidative stress and transforming growth factor-β (TGF-β) pathways have been implicated in endothelial cell loss and endothelial to mesenchymal transition of CECs in FECD. Ascorbic acid (AA) is found at high concentrations in FECD and its impact on CEC survival has been investigated. However, how TGF-β and AA effect the composition and rigidity of the CEC's matrix remains unknown.

Methods: In this study, we investigated the effect of AA, TGF-β1 and TGF-β3 on the deposition, ultrastructure, stiffness, and composition of the extracellular matrix (ECM) secreted by primary bovine corneal endothelial cells (BCECs).

*Corresponding author Vijaykrishna.raghunathan@gmail.com, smthomasy@ucdavis.edu.

Results: Immunofluorescence and electron microscopy post-decellularization demonstrated a robust deposition and distinct structure of ECM in response to treatments. AFM measurements showed that the modulus of the matrix in BCECs treated with TGF-β1 and TGF-β3 was significantly lower than the controls. There was no difference in the stiffness of the matrix between the AA-treated cell and controls. Gene Ontology analysis of the proteomics results revealed that AA modulates the oxidative stress pathway in the matrix while TGF-β induces the expression of matrix proteins collagen IV, laminin, and lysyl oxidase homolog 1.

Conclusions: Molecular pathways identified in this study demonstrate the differential role of soluble factors in the pathogenesis of FECD.

Keywords

Extracellular matrix (ECM); Fuchs endothelial corneal dystrophy (FECD); Atomic force microscopy (AFM); Proteomics; Ascorbic acid; Transforming growth factor- β

1. INTRODUCTION

The corneal endothelium is a metabolically active layer that acts as a critical barrier and pump to maintain a deturgescent state within the corneal stroma allowing for transparency. Loss of the barrier function leading to loss of endothelial cells (CECs), corneal edema, and opacity is a hallmark of corneal endothelial dystrophies like Fuchs endothelial corneal dystrophy (FECD) that is primary resolved through corneal transplantation (Cross et al., 1971; Mustonen et al., 1998). Progressive loss of CECs in FECD is associated with significant changes in the Descemet's membrane (DM), both at molecular and structural levels, with increased occurrence of excrescences (often rich in matrix/matricellular proteins) called guttae. Further, with late-onset of FECD, marked thickening of the DM is observed with interspersed layers of wide-spaced collagens (Bourne et al., 1982; Levy et al., 1996), primarily due to excessive production of extracellular matrix (ECM) proteins: collagen IV, fibronectin, and laminin by the CECs (Gottsch et al., 2005b; Weller et al., 2014). Such changes in the DM in FECD alter the biomecha(Ali et al., 2016)nical environment via tissue softening, in comparison with normal healthy individuals (Xia et al., 2016). More recently, using an early onset FECD model, we demonstrated softening of the DM in Col8a2 mutant mice preceded loss of CECs suggesting a role for the ECM in the pathology (Leonard et al., 2019). Changes in these biomechanical properties are purported to be accompanied by biochemical, compositional, and morphological alterations to the DM that are capable of markedly regulating subsequent cellular behavior and fate (Ali et al., 2016). It is thus imperative to understand bidirectional CEC-ECM interactions in the context of etiology and progression of FECD. A number of factors may play a role in altering the cellular microenvironment.

FECD has been associated with several genetic mutations and cellular pathways linked to dysfunctions in the ECM, oxidative stress, RNA toxicity, and cellular transdifferentiation. For example, mutations in genes encoding collagen (Col8A2), laminin subunit gamma 1 (LAMC1), transcription factors TCF4 and ZEB1, sodium borate transporter (SLC4A11), glutamate decarboxylase (AGBL1), lipoxygenase homology domain 1 (LOXHD1), and myotonic dystrophy type 1 protein kinase (DMPK) are strongly associated with FECD

(Afshari et al., 2017; Baratz et al., 2010; Desir et al., 2007; Gottsch et al., 2003; Gottsch et al., 2005a; Liskova et al., 2007; Mootha et al., 2017; Riazuddin et al., 2012; Vincent et al., 2009). However, the frequency of these mutations as well as their clinical presentation vary among different populations suggesting that FECD is a multifactorial condition with dysregulation of various signaling pathways reflecting the complexity of the pathology (Magovern et al., 1979; Nanda and Alone, 2019; Rosenblum et al., 1980; Wilson and Bourne, 1988; Zhang et al., 2006).

Multiple cellular pathways such as endothelial to mesenchymal transition (EnMT) RNA toxicity, oxidative stress, and apoptosis contribute to endothelial cell loss in FECD (Gottsch et al., 2003; Goyer et al., 2018; Nanda and Alone, 2019). Specifically, EnMT contributes to disease progression by modifying the ECM through altered deposition and remodeling of multiple collagen isoforms (I, III and XVI), fibronectin, and agrin in the DM (Goyer et al., 2018; Weller et al., 2014). Transforming growth factor-β (TGF-β) superfamily, specifically TGF-β1 and TGF-β3 isoforms, have been implicated to perturb cell signaling and to remodel the underlying matrix (DM) of CECs in progression of FECD (Reneker et al., 2010; Tandon et al., 2010). Activation of the TGF-β pathway results in EnMT, redox imbalance, oxidative stress, increased production of ECM proteins (e.g. laminin, fibronectin) and matrix remodeling, and inhibition of cell growth (Liu and Desai, 2015; Liu and Pravia, 2010; Okumura et al., 2017; Okumura et al., 2013; Pozzer et al., 2017; Usui et al., 1998; Wipff et al., 2007). Prolonged exposure to activated TGF-β leads to intracellular accumulation of ECM proteins and induction of the unfolded protein response (UPR). This process ultimately triggers endoplasmic reticular (ER) stress, leading to apoptosis and CEC loss (Okumura et al., 2017; Okumura et al., 2013) thus exacerbating the pathology.

Ascorbic acid (AA), a potent antioxidant and cyto-protectant found in high concentrations in the aqueous humor of the mammals (Reiss et al., 1986; Ringvold et al., 1998), has been shown to promote cell survival by enhancing the regenerative capacity in CECs derived from animals and humans *in vitro* (Jurkunas et al., 2010; Kim et al., 2017; Shima et al., 2011), likely by ameliorating oxidative stress (Jurkunas et al., 2010; Kim et al., 2017; Shima et al., 2011). Although AA is recognized as a potent antioxidant, it is also capable of stimulating ECM production in several cell types (Choi et al., 2008; Franceschi et al., 1994; Hata and Senoo, 1989; Tagler et al., 2014), including corneal stromal cells (Ren et al., 2008). It is thus evident that pro-inflammatory/pro-fibrotic cytokines (e.g., TGFβ) and antioxidants (e.g., AA) are both capable of modulating ECM deposition; how these matrices differ in composition, morphology, or biomechanics remain to be seen.

Ascertaining causal effects of AA or TGF-β on matrix remodeling using *in vivo* models are difficult to interpret. Thus, *in vitro* models such as ECM deposition by cells in culture, termed as cell derived matrices (CDM), present a viable alternative. The complex, organized mixture of macromolecules (structural and otherwise) presented by CDM *in vitro* partly mimic the extracellular microenvironment found *in vivo* and may be utilized to study cell-ECM interactions and delineate the specific roles that cells or ECM play in the pathology (Vlodavsky, 2001; Yamada and Cukierman, 2007). Since matrices differ by cell type, to understand FECD, is imperative that primary CECs are utilized *in vitro*. Primary human CECs are often isolated from donor corneal tissues deemed unsuitable for transplant; the

primary cause for rejection is low endothelial cell count with unknown etiology. This combined with an absence of donor ocular history presents an interesting challenge in knowing if the CECs isolated are truly normal. Thus, alternative sources, such as bovine or porcine, may be essential.

In this study we utilized primary CECs isolated from bovine eyes (BCECs) to investigate the effect of AA (cytoprotectant to oxidative stress) and TGF-β isoforms (TGF-β1 and TGF-β3; EnMT simulants) on the ECM protein deposition, structure, stiffness, and composition (Fig. 1). We hypothesized that similar to observed reports, EnMT simulants would result in softening of the cell derived matrix with associated changes in matricellular proteins contributing to pathology, while AA would have minimal effect and may secrete matricellular proteins that help alleviate oxidative stress. Together we posited that such an approach would be an important tool to study molecular mechanisms underlying FCED. In doing so, we were able to connect how these soluble factors modulate ECM composition and influence its rigidity. Finally, through quantitative proteomic analysis, we further correlated these findings with distinct cell signaling pathways to provide new insights into how AA and TGF-β influence the ECM of the cells. More importantly, we anticipate that generation of bovine CEC-derived ECM would be an important tool to study molecular mechanisms underlying the bidirectional interactions between CECs and their microenvironment in the context of FCED.

2. MATERIAL AND METHODS

2.1 Antibodies and Reagents

Pan-collagen (ab24117) and fibronectin (ab6584) antibodies were purchased from Abcam. Fluorophore conjugated phalloidin (A12380) was purchased from Life Technologies. Dulbecco's Phosphate-Buffered Saline (DPBS), Hank's Balanced Salt Solution (HBSS) and low glucose DMEM media (Hyclone) were obtained from GE healthcare life sciences. Fetal bovine serum (S11050H) was procured from Atlanta Biologicals™. TrypLE™ Express solution and gentamicin were purchased from Gibco. Penicillin-Streptomycin-Amphotericin (PSA) mixture was obtained from Lonza.

2.2 Isolation of bovine corneal endothelial cell line (BCECs)

Fresh bovine whole globes were obtained within 24 hours of euthanasia from Sierra for Medical Sciences (Whittier, CA). To isolate primary BCECs, the extraocular muscles and periocular tissues were removed from the globes by dissection. Eye globes were rinsed once in sterile PBS and then the cornea was excised at the limbus and before the start of the scleral line. Harvested corneas were placed endothelial side up in 12-well plates (Corning inc., NY) and soaked for 20 mins in sterile PBS containing 1% PSA and 0.5% Gentamicin. Afterwards, 300 μl of TrypLE™ Express solution was applied to the endothelial side of each cornea and corneas were incubated for another 20 mins at 37 °C and 5% CO_2. Following incubation, the endothelial side of each cornea was gently rubbed with a soft cell scraper. Dislodged primary cells were pooled into a 15 ml tube (collected cells from 10 corneas were pooled into one tube). Cells were centrifuged at 250×g for 5 mins. Supernatant was aspirated and pellet was re-suspended in Low Glucose DMEM containing 10% FBS, 1% PSA and

0.5% Gentamicin. Cells were then plated in 25 cm^2 flasks and were fed with fresh media every 3 days until they became confluent. Cells from three to five independent preparations were utilized for all experiments described in this study below.

2.3 ECM deposition by BCECs

ECM deposition was conducted on glass slides (VWR VistaVision™) and rounded coverslips (TED PELLA, Inc). Glass substrates were functionalized with amine groups to enhance cell/ECM adhesion as described elsewhere (Yemanyi et al., 2020b). Briefly, glass was coated with 3-aminopropyl trimethoxysaline (Sigma Aldrich, MO) overnight using a vacuum desiccator. Coated slides then were placed in an oven and were baked at 200 °C for 20 mins. Slides were sterilized with direct UV light for at least 45 mins in cell culture cabinet and each glass slide was placed in a 4-well plate (Thermo Scientific) for proteomics. For immunocytochemistry and AFM, round coverslips (10 mm) were placed in 24-well plates (Thermo Scientific). Primary BCECs at a density of 2.5×10^6 cells and 2×10^5 cells were seeded on glass slides and coverslips, respectively, and incubated for 24 hours at 37 °C and 5% CO_2. Cells were either untreated (control) or were treated with TGF-β1 (1 ng/ml), TGF-β3 (1 ng/ml), and ascorbic acid (AA) (50 μg/ml) twice a week for 6 weeks, following which cell derived matrices were obtained. To induce matrix production by the CECs, various concentrations of the TGF-β (0 ng/ml-100 ng/ml) has been used, (Usui et al., 1998) but TGF-β at a concentration of ≥1 μg/ml can be toxic to both the cornea and CECs (Liang et al., 1996). Therefore, to minimize the toxicity effects and to induce matrix production, a concentration of 1 ng/ml was chosen for this study. AA at concentrations between 10 to 265 μg/ml showed a very low toxicity when tested on the growth rate of CECs obtained from different species (Proulx et al., 2007; Shima et al., 2011). Therefore, AA at a concentration of 50 μg/ml was selected for this study.

2.4 Decellularization and ECM harvesting

Prior to decellularization, media was removed from each slide and washed twice with HBSS. Decellularization was performed as described previously (Yemanyi et al., 2020a). Briefly, slides were serially incubated 5 times with 20mM NH_4OH solution containing 0.05% Trition X-100. Afterwards, slides were washed 5 times with HBSS. The efficiency of decellularization was confirmed immediately by light microscopy and subsequently by immunocytochemistry. For proteomic analysis, decellularized glass slides were incubated with ECM extraction buffer (4 M guanidine hydrochloride, 10 mM dithiothreitol (DTT), 1:1000 DNAse I (0.05-0.375 U/μl) and 1:100 Halt protease inhibitor cocktail (Thermo Scientific)) for 3 minutes on ice and then samples were scraped into a 1.5 ml Eppendorf tubes. Samples were stored at −80°C until submitted to UC Davis Proteomics Core for analysis.

2.5 Immunocytochemistry

Samples prior to and after decellularization were fixed with 4% formaldehyde for 20 mins at room temperature. Afterwards, both samples were gently washed twice with PBS. Samples that were not decellularized were permeabilized with 0.1% Triton X-100 for 5 mins at room temperature. All samples were then washed once with PBS and then blocked in blocking buffer (10% [v/v] FBS/10% [v/v] SuperBlock in PBS) for 1 hour at 37°C.

Coverslips were then washed 3 times with PBS and incubated with primary pan-collagen or fibronectin antibodies for 1 hour at 37°C. Samples were then washed 3 times with PBS and incubated with species appropriate secondary antibody for another hour at 37°C. Following the incubation with secondary antibody, samples were washed with PBS for 3 times. To label F-actin, samples were incubated with Alexa Fluor-568 conjugated Phalloidin for 60 min at room temperature in the dark. Following incubation, samples were washed in PBS and counter stained with DAPI (0.5 μg/ml) for 5 minutes at room temperature. Slides were washed again with sterile PBS and mounted on a glass slides using Mowiol (an aqueous mounting medium comprised of polyvinyl alcohol and glycerol made in 0.2M Tris-Cl buffer (pH 8.5); DABCO (1,4-diazabicyclo-[2,2,2]-octane) was used as anti-fade) as the mounting medium.

2.6 Scanning electron microscopy (SEM)

Decellularized coverslips of controls and treated samples were fixed in Karnovsky's fixative for at least 1 week. The samples were rinsed with 0.1M phosphate buffer and then post-fixed for 2 hours in 1% buffered osmium tetroxide. Dehydration was initiated through ascending concentrations of ethanol with three changes of 100% and transitioned 1:1 with propylene oxide and completed using two changes of pure propylene oxide. Critically point dried samples were then mounted on stubs and coated with gold using sputter coater (Pelco Sputter Coater SC-7, Ted Pella Inc., CA). SEM images were taken at the UC Davis Biological Core Facility using Philips XL30 instrument.

2.7 Atomic force microscopy on ECM

Atomic force microscopy (AFM) was used to measure the mechanical properties of the ECM from four independent experiments/BCEC-derived ECM preparations. Briefly, force versus indentation curves were obtained using the MFP-3D Bio AFM (Asylum Research, Santa Barbara, CA) mounted on a Zeiss Axio Observer inverted microscope (Carl Zeiss, Thornwood, NY). To functionalize the cantilever, a dry borosilicate glass bead with a nominal radius of 4.9-5.6 μm (Thermo Scientific, Fremont, CA) was glued to the end of a silicon nitride PNP-TR-50 cantilever with calibrated spring constant (κ) of 55-246 pN nm^{-1} and length of 100 μm (Nano World, Switzerland). Deflection sensitivity of the probes was measured by taking the average of five force curves on a glass slide in DPBS immediately before the experimental samples. The spring constant of each cantilever probe used for the indentation measurements was determined using a thermal tuning method. To measure the stiffness of the ECM, freshly decellularized coverslips were adhered to the AFM dishes using cyanoacrylate glue. All samples were equilibrated in HBSS for at least 60 min prior to obtaining measurements to minimize thermal drift. For all samples, five force curves at 2 μm s^{-1} were obtained from 5-10 random positions. Elastic modulus (E) of each sample was obtained by fitting the indentation force vs. the indentation depth of the sample and further by applying the Hertz model for a spherical indenter, as shown in Eq. (1),

$$F = \frac{4}{3}\frac{E}{(1-\nu^2)}\sqrt{\delta^{3/2}\mathrm{R}}$$

Eq. 1

where F is the force applied by the indenter, E is Young's modulus, ν is Poisson's ratio (assumed to be 0.5 for biological samples (Herrmann, 1965)), δ is the indentation depth, and R is the radius of the borosilicate bead.

2.8 Protein extraction for proteomics

Bradford assay (Thermo Scientific) was performed to determine protein concentration of ECM extracts from five independent primary BCEC-derived preparations/experiments for all treatment groups. Proteins were precipitated and roughly 150 μg of protein was used for trypsin digestion. Pellets were solubilized in 100 μl of 6 M urea, 200 mM of dithiothreitol (DTT) was added to a final concentration of 5 mM and samples were incubated for 30 min at 37°C. Next, 20 mM iodoacetamide (IAA) was added to a final concentration of 15 mM and incubated for 30 min at room temperature, followed by the addition of 20 μL DTT to quench the IAA. Lys-C (Lysyl Endopeptidase, Wako Chemicals USA) was added to the sample and incubated for 2 hours at 30°C. Samples were then diluted to >1M urea by the addition of 50 mM AMBIC (ammonium bicarbonate), trypsin was added and digested overnight at 37°C. The following day, samples were desalted using Macro Spin Column (Nest Group).

2.8.1 Tandem Mass Tag (TMT) 10plex labeling—Desalted peptides were reconstituted in 30 μl of 50 mM TEAB (Tri Ethyl Ammonium Bicarbonate) and quantified using Pierce Fluorescent Peptide assay (Thermo Scientific). Each sample was diluted with 50 mM TEAB to 0.40 μg/μl; 10 μg of peptide was used per replicate. Samples were labeled using 10plex Tandem Mass Tag (TMT) Labeling Kits (Thermo Scientific). Briefly 20 μl of each TMT label (126N-131N) was added to each digested peptide sample and incubated for one hour. The reaction was quenched with 1 μl of 5% hydroxylamine and incubated for 15 minutes. A pooled sample was created by taking 1μg of all 20 samples (20 μg total) and then split into two 10 μg aliquots. Each pooled sample was labeled with the TMT 11 plex (131C) reagent and added to the two separate TMT 10 Plex experiments. All labeled samples were then mixed together in two sets of 11 samples and lyophilized to near dryness. TMT labeled samples were reconstituted in 0 .1% TFA and the pH was adjusted to 2 with 10% HCl. The combined sample (20 μg) was separated into 8 fractions by Pierce High-pH Reverse-Phase Peptide Fractionation kit (Thermo Scientific) with an extra wash before separation to remove extra TMT label reagent. The eight fractions were dried almost to completion.

2.8.2 LC-MS/MS—LC separation was done on a Dionex nano Ultimate 3000 (Thermo Fisher Scientific) with a Thermo Easy-Spray source. The digested peptides were reconstituted in 2% acetonitrile/0.1% trifluoroacetic acid and 5 μl of each sample was loaded onto a PepMap 100Å 3U 75 um x 20 mm reverse phase trap where they were desalted online before being separated on a 100 Å 2U 50-micron x 150 mm PepMap EasySpray reverse phase column. Peptides were eluted using a 180-minute gradient of 0.1% formic acid (A) and 80% acetonitrile (B) with a flow rate of 200 nL/min. The separation gradient was 2% to 5% B over 1 minute, 5% to 10% B over 9 minutes, 10% to 20% B over for 27 minutes, 20% to 35% B over 10 minutes, 35%B to 99%B over 10 minutes, a 2 minute hold at 99%B, and finally 99% B to 2%B held at 2% B for 5 minutes.

2.8.3 MS3 synchronous precursor selection workflow—Mass spectra were collected on a Fusion Lumos mass spectrometer (Thermo Fisher Scientific) in a data dependent MS3 synchronous precursor selection (SPS) method. MS1 spectra were acquired in the Orbitrap: 120K resolution, 50ms max inject time, and 5 x 10^5 AGC target. MS2 spectra were acquired in the linear ion trap with a 0.7 Da isolation window, CID fragmentation energy of 35%, turbo scan speed, 50 ms max inject time, 1 x 10^4 AGC target, and maximum parallelizable time turned on. MS2 ions were isolated in the ion trap and fragmented with a HCD energy of 65%. MS3 spectra were acquired in the Orbitrap with a resolution of 50K, a scan range of 100-500 Da, 105 ms max inject time, and 1 x 10^5 AGC target.

2.8.4 TMT IRS normalization and data analysis—RAW data files were processed and quantitated as previously described (Plubell et al., 2017). Briefly, raw files were processed with Proteome Discoverer 2.2 (Thermo Scientific) using the default MS3 SPS method with the following quantitative settings. Intensity was used for the TMT quantification and no normalization, imputation, or scaling was applied. All MS/MS samples were analyzed using Sequest HT to search all canonical Bovine sequences from Uniprot and 110 common laboratory contaminants (http://thegpm.org) plus an equal number of reverse decoy sequences assuming the digestion enzyme trypsin. Sequest-HT was searched with a fragment ion mass tolerance of 0.20 Da and a parent ion tolerance of 10.0 PPM. Carbamidomethyl of cysteine and TMT6plex of lysine were specified in Sequest-HT as fixed modifications. Oxidation of methionine and acetyl of the n-terminus were specified in Sequest-HT as variable modifications. Q-values computed by Percolator(Käll et al., 2007) were used to assign peptide confidence.

The default proteome discoverer PSM export report was processed using the PAWS pipeline modified for TMT quantitation (Wilmarth et al., 2009). This was used for inferring proteins, filtering (min intensity = 500, Perolator q-value = 5%, min 2 peptides per protein) and summing SPS MS3 reporter ion intensity (from unique peptides) to the protein level. Output from PAWS was analyzed using R to calculate the IRS normalized total reporter ion intensities and groups were compared with each other and to the controls using edgeR(Robinson et al., 2010).

2.8.5 Quantitative proteomics data analysis—GraphPad Prism was used to calculate differential expression of the found proteins for each condition from five independent experiments. Multiple *t*-tests and a stringent 5% false discovery cutoff was used to for each treatment. Identified proteins and their genes were used to further classify their molecular activity and their biological pathways. Gene classification, molecular function, and protein pathway analysis was conducted using Protein ANalysis THrough Evolutionary Relationships (PANTHER) classification system (http://www.pantherdb.org, version 13.1) (Mi et al., 2013; Thomas et al., 2003).

2.9 Image and Statistical analysis

Fluorescent intensity of the immunostained ECM were quantified using ImageJ (NIH). Graphs were compiled using GraphPad Prism 8 software for Windows (GraphPad Software,

Inc; La Jolla, CA). Results are expressed as means ± standard deviation (S. D). Elastic moduli values obtained from approximately 30 data points each from four independent experiments were represented as SuperPlots (Lord et al., 2020) to demonstrate variability and data spread. Differences between each treatment were compared using one-way ANOVA followed by Tukey's multiple comparison test in GraphPad Prism 8 software with $P < 0.05$ considered significant.

3. RESULTS

3.1 Structure and morphology of ECM in response to AA, TGF-β1 and TGF-β3

Immunostaining performed on samples prior to decellularization showed a uniform layer of hexagonal endothelial cells in all groups: control and those treated with AA or TGF-β1/TGF-β3 (Fig. 2). Efficiency of the decellularization was confirmed with all the samples co-stained with phalloidin and DAPI. No DAPI or F-actin was detected after decellularization suggesting efficient removal of cellular material. Deposition of ECM in response to AA and TGF-β was confirmed by immunostaining for pan-collagen and fibronectin, major components of the ECM (Fig. 2). Immunostained ECM images showed small yet significant differences in fluorescent intensities of collagen between control and AA treated samples; no differences were observed with TGF-β1/3 treatments. By contrast, TGF-β1/3 treatment resulted in significantly increased immunostaining of fibronectin that was not present with AA treatment compared with control groups. SEM images were obtained to document differences (if any) in ultrastructural features of the matrix between the controls, AA-, and TGF-β-treated samples; no obvious differences were observed between the samples. (Fig. 3).

3.2 The effect of TGF-β and AA on the mechanical properties of the ECM

AFM was used to determine the impact of AA, TGF-β1 and TGF-β3 on the mechanical properties of ECM produced by BCECs (Fig. 4). Our AFM results demonstrated that the ECMs of the BCECs treated with TGF-β1 (0.77 ± 0.3 kPa) and TGF-β3 (0.87 ± 0.4 kPa) were significantly softer than the ECM produced by the untreated BCECs (1.18 ± 0.4 kPa, $p < 0.05$) or AA treated BCECs (1.16 ± 0.5 kPa, $p < 0.05$). No statistically significant differences were seen comparing TGF-β1 and TGF-β3 (n=4 independent experiments; one-way ANOVA followed by Tukey's multiple comparison, $p = 0.28$), or between AA and control treated groups (n=4 independent experiments; one-way ANOVA followed by Tukey's multiple comparison, $p = 0.98$) (Fig. 4).

3.3 Abundance and distribution of ECM-associated proteins

Another method to evaluate the effects of AA, TGF-β1, and TGF-β3 on the composition of the ECM produced by BCECs was comparing the relative protein abundances between treatments using tandem mass tag (TMT) labelling and LC-MS/MS analysis. Untreated samples served as the control. A total of 2997 proteins were quantified from all samples (n = 5 for each treatment for a total of 20 samples). To detect differentially abundant proteins between the treatments, the Bioconductor package edgeR was used to perform statistical analysis of protein expression with a false discovery rate (FDR) of 5%. We identified that 32 proteins are differentially expressed between the controls and TGF-β1 treated

samples (Supplementary table 1). For TGF-β3, 69 differentially expressed proteins were found (Supplementary table 2). The highest numbers of differentially expressed proteins (Supplementary table 3) were observed between the controls and AA-treated samples.

The level of reproducibility between biological replicates of each treatment was evaluated using pair-wise scatter plots and correlation coefficients. Our generated data demonstrated a high level of reproducibility between the biological replicates in treated and untreated groups (Supplementary Fig 1 A-D). The differential abundance analysis resulted in many proteins with highly significant p-values (FDR < 0.05) and larger fold changes (Figure 5). This shows that treatment of BCECs with AA or TGF-β produced differential abundance changes in many ECM and ECM-bound proteins.

3.4 Differential expression of identified proteins

To profile differentially abundant proteins, TMT-labelled peptides were analyzed with LC-MS/MS to generate reporter ions for each biological sample. Proteins were tested for abundance differences using the exact test in edgeR and were considered significant if their FDR was less than 0.05. To classify the biological and physiological significance as well as biological pathways of the identified proteins, Gene Ontology PANTHER classification system was used. Gene symbols (from UniProt) for differentially abundant bovine proteins were used in PANTHER for categorization of their functional pathways.

AA-treated samples showed 12 distinct biological process pathways compared to 8 pathways for TGF-β1 and 10 pathways for TGF-β3 treated samples (Fig. 6 A, D & F). In AA-treated samples, “Cellular Process” showed the highest enrichment (33%) for Biological Process terms followed by “Metabolic Process” (20.4%) and “Localization” (12.6%) (Fig. 6 A). “Cellular Process” was also the most enriched Biological Process term in both TGF-β1 and TGF-β3-treated samples (52.6% for TGF-β1 and 44.8% for TGF-β3).

Further analysis of the cellular and metabolic process pathways in AA-treated cells revealed multiple biochemical pathways related to the ECM of the BCECs (Fig. 6 B & C). Categories and functions of proteins are highly different between the cellular and metabolic pathways, indicating the dynamics and variety of biochemical pathways involved in the ECM-derived BCECs in response to AA (Fig. 6 B & C).

Since “Cellular Process” was the most enriched term in both TGF-β1- and TGF-β3-treated samples, we further broke down this pathway (Fig. 6 E & G). Gene Ontology showed that the number of “Cellular Process” proteins in TGF-β1-treated sample was 24, compared to 64 for TGF-β3, simply showing that ECM of the BCECs in the presence of TGF-β3 was more dynamic compared to the ECM in the presence of TGF-β1 (Fig. 6 E & G). Further, ECM of the TGF-β3-treated samples showed more diverse biochemical pathways compared to the ECM of the TGF-β1-treated samples. Gene Ontology analysis of the identified genes revealed differential expression levels and a diverse network of biochemical pathways in the ECM of the treated samples, which can be used to define their specific role in pathogenesis of the corneal endothelial cells.

3.5 Molecular functions of the ECM proteins is specific to AA and TGF-β

We used PANTHER Gene Ontology function/pathway enrichment analysis to investigate the biological processes for the differentially abundant proteins in each treatment (Figure 7 A-C). Enrichment analysis showed a distinct pattern of molecular activity for each treated sample. ECM of the AA-treated cells had the highest amount of catalytic activity (34.6%) compared to TGF-β1 and TGF-β3-treated samples (14.3% and 23.3%, respectively). By contrast, both TGF-β1 and TGF-β3-treated samples showed an elevated activity of the structural molecules compared to AA-treated samples (25% and 19% versus 11% for AA), indicating that TGF-β tend to promote molecular pathways with activity that enhances the production of the ECM in BCECs.

Biological pathways of the differentially abundant proteins were analyzed using PANTHER Gene Ontology (Fig. 8 A-G). Compared to AA-treated samples, the number of identified pathways were more limited in both TGF-β1- and TGF-β3-treated samples (Fig. 8 A, D & F). Interestingly, in all the treated samples, integrin signaling was found to be the most common pathway among the identified pathways (Fig. 8 A, D & F). In ECM of the AA-treated BCECs, the inflammation pathway was the second most common pathway while, in ECM of the TGF-β1- and TGF-β3-treated cells, blood coagulation pathway was found to be the second most common pathway (31.6% for TGF-β1 and 16.7% for TGF-β3).

Further analysis of the integrin signaling pathway in AA-treated cells revealed that 62% of the pathway was represented by collagen and collagen related proteins followed by laminin, which was found to be around 20% (Fig. 8 B). Although the analysis of AA-related inflammation pathway revealed different biochemical pathways, it showed that 42% of the pathways belonged to ECM proteins (Fig. 8 C). Differential analysis of the integrin signaling pathway in the ECM of the BCECs treated with TGF-β1 and TGF-β3 showed that almost all the pathway is dominated by ECM proteins. For TGF-β1-treated samples, collagen was found to be the highest contributing ECM protein (57.1%) followed by laminin (42.9%). For TGF-β3 treated samples a similar trend was observed with collagen being the most abundant (58.3%) followed by laminin and fibronectin (25% and 16.7%, respectively). Differential analysis of the expressed proteins in dominant pathways revealed the central role of the ECM in maintaining the physiological functions of cells.

Among the classified proteins in AA-treated samples, we identified those that are specifically implicated in oxidative stress. Based on the protein *p*-value, we discovered a significant upregulation in the expression of peroxiredoxin-1 (PRDX1) and glutathione peroxidase 8 (GPX8) but a downregulation in the expression of superoxide dismutase [Cu-Zn] (SOD3) (Table 1). In TGF-β3 treated samples, we found significant upregulation of 14 different matrix proteins such as various collagen IV isoforms, laminin, lysyl oxidase homolog 1, and metalloproteinase inhibitor 3 (please see Table 2 for the complete list). Surprisingly, compared to control, we did not detect any significant up- or down regulation of matrix proteins in the TGF-β1-treated samples.

4. DISCUSSION

In this study, we investigated the effect of AA and TGF-β on the organization, mechanical properties, and composition of the ECM derived by primary BCECs. Previous studies have shown fibroblast-like morphology and EnMT in human corneal endothelial cells following the TGF-β treatment (Okumura et al., 2013; Saika, 2006). However, we detected no morphological change in primary BCECs after the 6-week treatment period. BCECs maintained their hexagonal monolayer formation throughout the treatment period and their morphology was comparable to the control group. Since studies have shown that the ECM composition and proteins markedly change following the morphological change of the CECs (Okumura et al., 2013), maintaining the BCECs' original characteristics and physiological function was the crucial part of this study to avoid any misinterpretation.

4.1 Morphological and biomechanical characterization

Our SEM results revealed no obvious differences in the matrix of cells treated with AA and TGF-β1/3. However, we did observe subtle differences wherein ECM after control and TGFβ3 treatment appeared more sheet-like with pores, while ECM after AA and TGFβ1 treatment was more fibrillar. Additional studies are required to extensively quantify ECM organization using immunogold labeling and was deemed out of the scope of this study. It remains to be seen how localized and subtle differences in matrix ultrastructure contribute to progression of the FECD and CEC loss, if any. Immunostaining for fibronectin and collagen revealed important differences in response to TGF-β or AA, respectively. Specifically, AA appeared to increase collagen immunostaining, as expected(Franceschi et al., 1994; Hata and Senoo, 1989), while TGFβ facilitated fibronectin expression significantly. This is consistent with previous studies showing that TGF-β triggers excessive production of the ECM *in vitro*, a process that also induces fibrosis in various tissues such as lung (Roberts et al., 1986; Sime et al., 1997). The presence of fibronectin in the ECM enables recruitment of TGFβ and TGFβ induced protein to promote fibrosis, thus contributing to detrimental positive feedback (Kadler et al., 2008; Klingberg et al., 2018; Muro et al., 2008). Specifically, inhibition of fibronectin alleviates pro-fibrotic phenotypes in cells and tissues (Kohan et al., 2010; Valiente-Alandi et al., 2018). However, unlike other fibrotic models where TGFβ mediated ECM stiffening was observed (Wells, 2013), we observed that, surprisingly, for ECM secreted by TGF-β-treated cells were significantly softer than untreated control. Whilst this seemingly appears to contradict a previous observation from our group where TGFβ3 treated trabecular meshwork cells deposit a stiffer CDM (Raghunathan et al., 2015), this finding is in agreement with a previous study where the modulus of DM in FECD-affected patients were observed to be significantly lower compared to normal donors (Xia et al., 2016). This emphasizes the importance of studying ECM biomechanics and composition in a cell-type and context dependent manner.

Since BCECs maintained their hexagonal morphology despite chronic TGF-β treatment akin to what the cells may be exposed to *in vivo*, it is likely that changes observed in the ECM precede changes in cell morphology. Further, based on our observations, we speculate that softening in the ECM is likely due to disorganization of the structural proteins. Future studies would be required to document ultrastructural changes combining serial block face

scanning electron microscopy and immuno-gold labelling for target proteins to determine which structural components may play a causal role in ECM softening. Further, whether similar observations translate to ECM deposited by human primary CECs comparing non-FECD and FECD donors remain to be investigated.

4.2 Proteomic characterization

Another factor that contributes to matrix biomechanics is how these structural proteins may be crosslinked with each other. Lysyl oxidase (LOX) is a key ECM cross linker and is thought to play a defining role in mechanical properties of the matrix (Elbjeirami et al., 2003). Although we detected significant overexpression of lysyl oxidase homolog 1 (LOXL1) in TGF-β3 treated samples, its expression inversely correlated with a change in elastic modulus. Indeed, LOXL1 is identified as a downstream target of TGF-β1/2 signaling in ocular cell types (Sethi et al., 2011). Whether the elevated expression of LOXL1, as observed here, translates to either: increases in its enzymatic activity, or rendered inactive in our matrices, or if enzyme activity and kinetics differ with different TGF-β isoforms remains unclear. It is also unclear if the ECM has sufficient substrates/ligands for LOXL1 activity to be effective. Further, to the best of our knowledge, LOXL1 has not been implicated in FECD; thus, understanding LOX protein and its homologs in the context of CEC health and DM homeostasis warrants further investigation.

Our Gene Ontology analysis demonstrated that AA and TGF-β1/TGF-β3 isoforms modulate a vast array of metabolic and molecular pathways in the ECM. For instance, we found that AA and TGF-β1/TGF-β3 isoforms modulate the expression of the ECM molecules collagen, laminin, and fibronectin. We also found that TGF-β1 treatment resulted in elevated amounts of secreted frizzled related protein 1-(sFRP1) in BCEC ECM. sFRP1 is a non-canonical Wnt inhibitor. Interestingly, while upregulation of sFRP1 has been observed in other fibrotic diseases, sFRP1 was shown to be required for inhibition of severe organ damage through non-canonical Wnt/PCP pathway(Matsuyama et al., 2014). It is thus unclear if the increase in sFRP1 is cytoprotective or an adverse event. Another Wnt gene, WNT4, reported to be upregulated in FECD patients (Cui et al., 2018) and renal fibrosis(DiRocco et al., 2013) but downregulated with sensescence (Kvell et al., 2010), was demonstrated to be important for mesenchymal to epithelial transition(DiRocco et al., 2013; Taki et al., 2003). Studies have shown that Wnt signaling, independently or through interaction with other pathways, promotes expression and organization of ECM proteins (such as fibronectin), cell migration, and fibrosis (Brack et al., 2007; Dzamba et al., 2009; Nelson and Nusse, 2004; Tao et al., 2016). Whether Wnt signaling plays a critical role in FECD pathogenesis remains to be explored.

Oxidative stress and DNA damage followed by apoptosis are implicated in endothelial cell loss in FECD (Jurkunas et al., 2010; Kim et al., 2017). Interestingly, our proteomics results demonstrate an increase in expression of the Peroxiredoxin-1 (PRDX1) and glutathione peroxidase 8 (GPX8) in the ECM of the BCECs treated with AA, indicating that AA induces the expression of these antioxidants in CECs. One preliminary study has reported an upregulation of AA in aqueous humor of FECD patients (Gupta et al., 2017); this however has not been confirmed by additional studies. Nevertheless, ascorbic acid has

been postulated to ameliorate oxidative stress induced damage, reduce apoptosis, and promote proliferation in corneal endothelial cells (Hsueh et al., 2020; Hsueh et al., 2021) Together, these posit AA in FECD may be an adaptive response to facilitate production of antioxidants; we thus speculate that when this stress is prolonged and unsustainable, cells may no longer be able to rescue themselves. Randomized studies are required to determine the amounts and role of ascorbic acid in FECD. PRDX1 and GPX8 are known to be mostly active inside the cells. In fact, it is shown that expression of other PRDX isoforms, PRDX2 and PRDX6, is reduced in FECD endothelial cells compared to normal samples (Jurkunas et al., 2008). In addition to intracellular role of these antioxidants, recent studies have revealed the novel role of PRDX1 and GPX8 in the ECM of the cells (Bagulho et al., 2015; Kawai and Akira, 2010). PRDX1 secretion into the ECM triggers TLR4-mediated inflammation, immunity, and tissue repair responses (Bagulho et al., 2015; Kawai and Akira, 2010), a biochemical pathway that we found to be the second most upregulated pathway in AA-treated cells. Similarly, inflammatory and immune pathways have been found to be upregulated in late onset FECD (Cui et al., 2018). Thus, based on these findings, we speculate that AA initially promotes the expression of antioxidants in both CECs and ECM and that these molecules further induce a secondary inflammatory and immune response as a defense mechanism to avoid cell apoptosis. However, further mechanistic studies are essential to elucidate whether these pathways individually, or in coordination with each other, could potentially prevent endothelial cell from undergoing apoptosis.

In AA-treated ECM, we found a decrease in matrix-specific superoxide dismutase [Cu-Zn] (SOD3) expression in the ECM of the BCECs treated with AA, consistent with the recent study where down regulation of superoxide dismutase SOD2 and SOD3 was detected in CECs isolated from the FECD patients (Cui et al., 2018). Downregulation of SOD2/3 has been associated with upregulation of reactive oxygen species, cell apoptosis and senescence in CECs and FECD (Cui et al., 2018). Given the higher concentration of AA in aqueous humor of FECD patients, it remains to be investigated why SOD levels are downregulated in FECD. One possible explanation might be because of the overlapping functions of the SOD and AA (Tamari et al., 2013). Thus since AA is able to mimic the antioxidant function of the SOD1 and SOD2 in SOD knockout cells (Tamari et al., 2013), its presence may lead to downregulation of intra and extracellular SODs, modulation of the apoptosis and/or senescence, as an adaptive response. However, it is likely that beyond a critical level AA is insufficient to compensate for the loss or downregulation of various SOD isoforms, thus contributing to dysfunction in FECD.

In this study, we demonstrated that BCEC derived CDMs may be a potent tool to study ECM biology and CEC-matrix interactions in the context of FECD pathogenesis. Our data shows definitive biochemical and mechanical changes in the ECM of CECs, mediated by AA and TGF-β, that mirror observations in the DM of patients with FECD. This supports BCEC derived CDMs as a model system for studying etiology and progression of this disease.

5. LIMITATIONS

While we demonstrate that CDMs from BCECs may be a viable model to study CEC dysfunction, this study is not without limitations. First, we utilize bovine cells while

acknowledging the importance of developing *in vitro* or *in vivo* models in a species specific, context dependent, and disease relevant manner. Thus, further studies addressing the feasibility in primary human cells from non-FECD and FECD donors is vital. Next, we determined the effects of AA and TGFβ1/3 on select concentrations based on prior studies. Additional studies are required to determine if changes in the matrix observed are dose/time dependent. Also, cells here were cultured in media containing 10% serum. CECs natively are exposed to the aqueous humor whose protein content is <1% (Freddo, 2013). Future studies are required where cells are cultured in reduced serum conditions to mitigate serum effects. Finally, studies focused on quantifying morphometric and ultrastructural changes in CDMs are essential to comprehend the implications of a softer ECM.

Supplementary Material

Refer to Web version on PubMed Central for supplementary material.

ACKNOWLEDGMENTS

The authors would like to thank their funding sources: National Institutes of Health [grant numbers R01EY016134, R01EY019970, and P30EY12576]. P.A.W. was funded in part by NIH grant P30EY10572.

DATA AVAILABILITY

Raw data obtained for quantitative proteomics can be downloaded from MassIVE (https://massive.ucsd.edu/ProteoSAFe/static/massive.jsp) Dataset identifier # = MSV000088172, or Proteome Exchange (http://www.proteomexchange.org/) Dataset identifier # = PXD028868. An excel sheet with all proteins identified can be found in supplementary information.

REFERENCES

Afshari NA, Igo RP Jr., Morris NJ, Stambolian D, Sharma S, Pulagam VL, Dunn S, Stamler JF, Truitt BJ, Rimmler J, Kuot A, Croasdale CR, Qin X, Burdon KP, Riazuddin SA, Mills R, Klebe S, Minear MA, Zhao J, Balajonda E, Rosenwasser GO, Baratz KH, Mootha VV, Patel SV, Gregory SG, Bailey-Wilson JE, Price MO, Price FW Jr., Craig JE, Fingert JH, Gottsch JD, Aldave AJ, Klintworth GK, Lass JH, Li YJ, Iyengar SK, 2017. Genome-wide association study identifies three novel loci in Fuchs endothelial corneal dystrophy. Nat Commun 8, 14898. [PubMed: 28358029]

Ali M, Raghunathan V, Li JY, Murphy CJ, Thomasy SM, 2016. Biomechanical relationships between the corneal endothelium and Descemet's membrane. Exp. Eye Res 152, 57–70. [PubMed: 27639516]

Bagulho A, Vilas-Boas F, Pena A, Peneda C, Santos FC, Jeronimo A, de Almeida RFM, Real C, 2015. The extracellular matrix modulates H2O2 degradation and redox signaling in endothelial cells. Redox Biol 6, 454–460. [PubMed: 26409032]

Baratz KH, Tosakulwong N, Ryu E, Brown WL, Branham K, Chen W, Tran KD, Schmid-Kubista KE, Heckenlively JR, Swaroop A, Abecasis G, Bailey KR, Edwards AO, 2010. E2-2 protein and Fuchs's corneal dystrophy. N Engl J Med 363, 1016–1024. [PubMed: 20825314]

Bourne WM, Johnson DH, Campbell RJ, 1982. The ultrastructure of Descemet's membrane. III. Fuchs' dystrophy. Arch Ophthalmol 100, 1952–1955. [PubMed: 6983339]

Brack AS, Conboy MJ, Roy S, Lee M, Kuo CJ, Keller C, Rando TA, 2007. Increased Wnt signaling during aging alters muscle stem cell fate and increases fibrosis. Science 317, 807–810. [PubMed: 17690295]

Choi KM, Seo YK, Yoon HH, Song KY, Kwon SY, Lee HS, Park JK, 2008. Effect of ascorbic acid on bone marrow-derived mesenchymal stem cell proliferation and differentiation. J. Biosci. Bioeng 105, 586–594. [PubMed: 18640597]

Cross HE, Maumenee AE, Cantolino SJ, 1971. Inheritance of Fuchs' endothelial dystrophy. Arch Ophthalmol 85, 268–272. [PubMed: 5313141]

Cui Z, Zeng Q, Guo Y, Liu S, Wang P, Xie M, Chen J, 2018. Pathological molecular mechanism of symptomatic late-onset Fuchs endothelial corneal dystrophy by bioinformatic analysis. PLoS One 13, e0197750. [PubMed: 29787599]

Desir J, Moya G, Reish O, Van Regemorter N, Deconinck H, David KL, Meire FM, Abramowicz MJ, 2007. Borate transporter SLC4A11 mutations cause both Harboyan syndrome and non-syndromic corneal endothelial dystrophy. J Med Genet 44, 322–326. [PubMed: 17220209]

DiRocco DP, Kobayashi A, Taketo MM, McMahon AP, Humphreys BD, 2013. Wnt4/β–Catenin Signaling in Medullary Kidney Myofibroblasts. J. Am. Soc. Nephrol 24, 1399–1412. [PubMed: 23766539]

Dzamba BJ, Jakab KR, Marsden M, Schwartz MA, DeSimone DW, 2009. Cadherin adhesion, tissue tension, and noncanonical Wnt signaling regulate fibronectin matrix organization. Dev. Cell 16, 421–432. [PubMed: 19289087]

Elbjeirami WM, Yonter EO, Starcher BC, West JL, 2003. Enhancing mechanical properties of tissue-engineered constructs via lysyl oxidase crosslinking activity. J Biomed Mater Res A 66, 513–521. [PubMed: 12918034]

Franceschi RT, Iyer BS, Cui Y, 1994. Effects of ascorbic acid on collagen matrix formation and osteoblast differentiation in murine MC3T3-E1 cells. J. Bone Miner. Res 9, 843–854. [PubMed: 8079660]

Freddo TF, 2013. A contemporary concept of the blood-aqueous barrier. Prog. Retin. Eye Res 32, 181–195. [PubMed: 23128417]

Gottsch JD, Bowers AL, Margulies EH, Seitzman GD, Kim SW, Saha S, Jun AS, Stark WJ, Liu SH, 2003. Serial analysis of gene expression in the corneal endothelium of Fuchs' dystrophy. Invest. Ophthalmol. Vis. Sci 44, 594–599. [PubMed: 12556388]

Gottsch JD, Sundin OH, Liu SH, Jun AS, Broman KW, Stark WJ, Vito EC, Narang AK, Thompson JM, Magovern M, 2005a. Inheritance of a novel COL8A2 mutation defines a distinct early-onset subtype of fuchs corneal dystrophy. Invest. Ophthalmol. Vis. Sci 46, 1934–1939. [PubMed: 15914606]

Gottsch JD, Zhang C, Sundin OH, Bell WR, Stark WJ, Green WR, 2005b. Fuchs corneal dystrophy: aberrant collagen distribution in an L450W mutant of the COL8A2 gene. Invest Ophthalmol Vis Sci 46, 4504–4511. [PubMed: 16303941]

Goyer B, Theriault M, Gendron SP, Brunette I, Rochette PJ, Proulx S, 2018. Extracellular Matrix and Integrin Expression Profiles in Fuchs Endothelial Corneal Dystrophy Cells and Tissue Model. Tissue Eng Part A 24, 607–615. [PubMed: 28726551]

Gupta R, Ross AE, Ciolino JB, Vasanth S, Jurkunas UV, 2017. Ascorbic acid and hydrogen peroxide levels in the aqueous humor in Fuchs Endothelial Corneal Dystrophy. Investigative Ophthalmology & Visual Science 58, 1446–1446.

Hata R, Senoo H, 1989. L-ascorbic acid 2-phosphate stimulates collagen accumulation, cell proliferation, and formation of a three-dimensional tissuelike substance by skin fibroblasts. J. Cell. Physiol 138, 8–16. [PubMed: 2910890]

Herrmann LR, 1965. Elasticity Equations for Incompressible and Nearly Incompressible Materials by a Variational Theorem. AIAA J. 3, 1896-&.

Hsueh Y-J, Meir Y-JJ, Yeh L-K, Wang T-K, Huang C-C, Lu T-T, Cheng C-M, Wu W-C, Chen H-C, 2020. Topical Ascorbic Acid Ameliorates Oxidative Stress-Induced Corneal Endothelial Damage via Suppression of Apoptosis and Autophagic Flux Blockage. Cells 9, 943. [PubMed: 32290365]

Hsueh YJ, Meir YJ, Lai JY, Huang CC, Lu TT, Ma DH, Cheng CM, Wu WC, Chen HC, 2021. Ascorbic acid ameliorates corneal endothelial dysfunction and enhances cell proliferation via the noncanonical GLUT1-ERK axis. Biomed. Pharmacother 144, 112306. [PubMed: 34656060]

Jurkunas UV, Bitar MS, Funaki T, Azizi B, 2010. Evidence of oxidative stress in the pathogenesis of fuchs endothelial corneal dystrophy. Am J Pathol 177, 2278–2289. [PubMed: 20847286]

Jurkunas UV, Rawe I, Bitar MS, Zhu C, Harris DL, Colby K, Joyce NC, 2008. Decreased expression of peroxiredoxins in Fuchs' endothelial dystrophy. Invest. Ophthalmol. Vis. Sci 49, 2956–2963. [PubMed: 18378575]

Kadler KE, Hill A, Canty-Laird EG, 2008. Collagen fibrillogenesis: fibronectin, integrins, and minor collagens as organizers and nucleators. Curr. Opin. Cell Biol 20, 495–501. [PubMed: 18640274]

Käll L, Canterbury JD, Weston J, Noble WS, MacCoss MJ, 2007. Semi-supervised learning for peptide identification from shotgun proteomics datasets. Nat. Methods 4, 923–925. [PubMed: 17952086]

Kawai T, Akira S, 2010. The role of pattern-recognition receptors in innate immunity: update on Toll-like receptors. Nat Immunol 11, 373–384. [PubMed: 20404851]

Kim EC, Toyono T, Berlinicke CA, Zack DJ, Jurkunas U, Usui T, Jun AS, 2017. Screening and Characterization of Drugs That Protect Corneal Endothelial Cells Against Unfolded Protein Response and Oxidative Stress. Invest Ophthalmol Vis Sci 58, 892–900. [PubMed: 28159976]

Klingberg F, Chau G, Walraven M, Boo S, Koehler A, Chow ML, Olsen AL, Im M, Lodyga M, Wells RG, White ES, Hinz B, 2018. The fibronectin ED-A domain enhances recruitment of latent TGF-β-binding protein-1 to the fibroblast matrix. J. Cell Sci 131.

Kohan M, Muro AF, White ES, Berkman N, 2010. EDA-containing cellular fibronectin induces fibroblast differentiation through binding to alpha4beta7 integrin receptor and MAPK/Erk 1/2-dependent signaling. FASEB J. 24, 4503–4512. [PubMed: 20643910]

Kvell K, Varecza Z, Bartis D, Hesse S, Parnell S, Anderson G, Jenkinson EJ, Pongracz JE, 2010. Wnt4 and LAP2alpha as Pacemakers of Thymic Epithelial Senescence. PLoS One 5, e10701. [PubMed: 20502698]

Leonard BC, Jalilian I, Raghunathan VK, Wang W, Jun AS, Murphy CJ, Thomasy SM, 2019. Biomechanical changes to Descemet's membrane precede endothelial cell loss in an early-onset murine model of Fuchs endothelial corneal dystrophy. Exp. Eye Res 180, 18–22. [PubMed: 30471280]

Levy SG, Moss J, Sawada H, Dopping-Hepenstal PJ, McCartney AC, 1996. The composition of wide-spaced collagen in normal and diseased Descemet's membrane. Curr Eye Res 15, 45–52. [PubMed: 8631203]

Liang C, Peyman GA, Federman J, 1996. Ocular toxicity of intravitreous transforming growth factor-beta 1. Eye (Lond) 10 (Pt 6), 709–713. [PubMed: 9091367]

Liskova P, Tuft SJ, Gwilliam R, Ebenezer ND, Jirsova K, Prescott Q, Martincova R, Pretorius M, Sinclair N, Boase DL, Jeffrey MJ, Deloukas P, Hardcastle AJ, Filipec M, Bhattacharya SS, 2007. Novel mutations in the ZEB1 gene identified in Czech and British patients with posterior polymorphous corneal dystrophy. Hum. Mutat 28, 638.

Liu RM, Desai LP, 2015. Reciprocal regulation of TGF-beta and reactive oxygen species: A perverse cycle for fibrosis. Redox Biol 6, 565–577. [PubMed: 26496488]

Liu RM, Pravia KAG, 2010. Oxidative stress and glutathione in TGF-beta-mediated fibrogenesis. Free Radical Bio Med 48, 1–15. [PubMed: 19800967]

Lord SJ, Velle KB, Mullins RD, Fritz-Laylin LK, 2020. SuperPlots: Communicating reproducibility and variability in cell biology. Journal of Cell Biology 219.

Magovern M, Beauchamp GR, McTigue JW, Fine BS, Baumiller RC, 1979. Inheritance of Fuchs' combined dystrophy. Ophthalmology 86, 1897–1923. [PubMed: 399801]

Matsuyama M, Nomori A, Nakakuni K, Shimono A, Fukushima M, 2014. Secreted Frizzled-related Protein 1 (Sfrp1) Regulates the Progression of Renal Fibrosis in a Mouse Model of Obstructive Nephropathy *. J. Biol. Chem 289, 31526–31533. [PubMed: 25253698]

Mi H, Muruganujan A, Thomas PD, 2013. PANTHER in 2013: modeling the evolution of gene function, and other gene attributes, in the context of phylogenetic trees. Nucleic Acids Res 41, D377–386. [PubMed: 23193289]

Mootha VV, Hansen B, Rong Z, Mammen PP, Zhou Z, Xing C, Gong X, 2017. Fuchs' Endothelial Corneal Dystrophy and RNA Foci in Patients With Myotonic Dystrophy. Invest Ophthalmol Vis Sci 58, 4579–4585. [PubMed: 28886202]

Muro AF, Moretti FA, Moore BB, Yan M, Atrasz RG, Wilke CA, Flaherty KR, Martinez FJ, Tsui JL, Sheppard D, Baralle FE, Toews GB, White ES, 2008. An Essential Role for Fibronectin Extra

Type III Domain A in Pulmonary Fibrosis. Am. J. Respir. Crit. Care Med 177, 638–645. [PubMed: 18096707]

Mustonen RK, McDonald MB, Srivannaboon S, Tan AL, Doubrava MW, Kim CK, 1998. In vivo confocal microscopy of Fuchs' endothelial dystrophy. Cornea 17, 493–503. [PubMed: 9756443]

Nanda GG, Alone DP, 2019. REVIEW: Current understanding of the pathogenesis of Fuchs' endothelial corneal dystrophy. Mol Vis 25, 295–310. [PubMed: 31263352]

Nelson WJ, Nusse R, 2004. Convergence of Wnt, beta-catenin, and cadherin pathways. Science 303, 1483–1487. [PubMed: 15001769]

Okumura N, Hashimoto K, Kitahara M, Okuda H, Ueda E, Watanabe K, Nakahara M, Sato T, Kinoshita S, Tourtas T, Schlotzer-Schrehardt U, Kruse F, Koizumi N, 2017. Activation of TGF-beta signaling induces cell death via the unfolded protein response in Fuchs endothelial corneal dystrophy. Sci. Rep 7, 6801. [PubMed: 28754918]

Okumura N, Kay EP, Nakahara M, Hamuro J, Kinoshita S, Koizumi N, 2013. Inhibition of TGF-beta signaling enables human corneal endothelial cell expansion in vitro for use in regenerative medicine. PLoS One 8, e58000. [PubMed: 23451286]

Plubell DL, Wilmarth PA, Zhao Y, Fenton AM, Minnier J, Reddy AP, Klimek J, Yang X, David LL, Pamir N, 2017. Extended Multiplexing of Tandem Mass Tags (TMT) Labeling Reveals Age and High Fat Diet Specific Proteome Changes in Mouse Epididymal Adipose Tissue. Mol Cell Proteomics 16, 873–890. [PubMed: 28325852]

Pozzer D, Favellato M, Bolis M, Invernizzi RW, Solagna F, Blaauw B, Zito E, 2017. Endoplasmic Reticulum Oxidative Stress Triggers Tgf-Beta-Dependent Muscle Dysfunction by Accelerating Ascorbic Acid Turnover. Sci Rep 7, 40993. [PubMed: 28106121]

Proulx S, Bourget JM, Gagnon N, Martel S, Deschambeault A, Carrier P, Giasson CJ, Auger FA, Brunette I, Germain L, 2007. Optimization of culture conditions for porcine corneal endothelial cells. Mol Vis 13, 524–533. [PubMed: 17438517]

Raghunathan VK, Morgan JT, Chang YR, Weber D, Phinney B, Murphy CJ, Russell P, 2015. Transforming Growth Factor Beta 3 Modifies Mechanics and Composition of Extracellular Matrix Deposited by Human Trabecular Meshwork Cells. ACS Biomater Sci Eng 1, 110–118. [PubMed: 30882039]

Reiss GR, Werness PG, Zollman PE, Brubaker RF, 1986. Ascorbic acid levels in the aqueous humor of nocturnal and diurnal mammals. Arch Ophthalmol 104, 753–755. [PubMed: 3707416]

Ren R, Hutcheon AE, Guo XQ, Saeidi N, Melotti SA, Ruberti JW, Zieske JD, Trinkaus-Randall V, 2008. Human primary corneal fibroblasts synthesize and deposit proteoglycans in long-term 3-D cultures. Dev Dyn 237, 2705–2715. [PubMed: 18624285]

Reneker LW, Bloch A, Xie L, Overbeek PA, Ash JD, 2010. Induction of corneal myofibroblasts by lens-derived transforming growth factor beta1 (TGFbeta1): a transgenic mouse model. Brain Res Bull 81, 287–296. [PubMed: 19897021]

Riazuddin SA, Parker DS, McGlumphy EJ, Oh EC, Iliff BW, Schmedt T, Jurkunas U, Schleif R, Katsanis N, Gottsch JD, 2012. Mutations in LOXHD1, a recessive-deafness locus, cause dominant late-onset Fuchs corneal dystrophy. Am J Hum Genet 90, 533–539. [PubMed: 22341973]

Ringvold A, Anderssen E, Kjonniksen I, 1998. Ascorbate in the corneal epithelium of diurnal and nocturnal species. Invest Ophthalmol Vis Sci 39, 2774–2777. [PubMed: 9856789]

Roberts AB, Sporn MB, Assoian RK, Smith JM, Roche NS, Wakefield LM, Heine UI, Liotta LA, Falanga V, Kehrl JH, et al. , 1986. Transforming growth factor type beta: rapid induction of fibrosis and angiogenesis in vivo and stimulation of collagen formation in vitro. Proc Natl Acad Sci U S A 83, 4167–4171. [PubMed: 2424019]

Robinson MD, McCarthy DJ, Smyth GK, 2010. edgeR: a Bioconductor package for differential expression analysis of digital gene expression data. Bioinformatics 26, 139–140. [PubMed: 19910308]

Rosenblum P, Stark WJ, Maumenee IH, Hirst LW, Maumenee AE, 1980. Hereditary Fuchs' Dystrophy. Am J Ophthalmol 90, 455–462. [PubMed: 6968504]

Saika S., 2006. TGFbeta pathobiology in the eye. Lab. Invest 86, 106–115. [PubMed: 16341020]

Sethi A, Mao W, Wordinger RJ, Clark AF, 2011. Transforming growth factor-beta induces extracellular matrix protein cross-linking lysyl oxidase (LOX) genes in human trabecular meshwork cells. Invest Ophthalmol Vis Sci 52, 5240–5250. [PubMed: 21546528]

Shima N, Kimoto M, Yamaguchi M, Yamagami S, 2011. Increased proliferation and replicative lifespan of isolated human corneal endothelial cells with L-ascorbic acid 2-phosphate. Invest Ophthalmol Vis Sci 52, 8711–8717. [PubMed: 21980003]

Sime PJ, Xing Z, Graham FL, Csaky KG, Gauldie J, 1997. Adenovector-mediated gene transfer of active transforming growth factor-beta1 induces prolonged severe fibrosis in rat lung. J Clin Invest 100, 768–776. [PubMed: 9259574]

Tagler D, Makanji Y, Tu T, Bernabe BP, Lee R, Zhu J, Kniazeva E, Hornick JE, Woodruff TK, Shea LD, 2014. Promoting extracellular matrix remodeling via ascorbic acid enhances the survival of primary ovarian follicles encapsulated in alginate hydrogels. Biotechnol. Bioeng 111, 1417–1429. [PubMed: 24375265]

Taki M, Kamata N, Yokoyama K, Fujimoto R, Tsutsumi S, Nagayama M, 2003. Downregulation of Wnt4 and upregulation of Wnt5a expression by epithelialmesenchymal transition in human squamous carcinoma cells. Cancer Sci. 94, 593–597. [PubMed: 12841867]

Tamari Y, Nawata H, Inoue E, Yoshimura A, Yoshii H, Kashino G, Seki M, Enomoto T, Watanabe M, Tano K, 2013. Protective roles of ascorbic acid in oxidative stress induced by depletion of superoxide dismutase in vertebrate cells. Free Radic Res 47, 1–7.

Tandon A, Tovey JC, Sharma A, Gupta R, Mohan RR, 2010. Role of transforming growth factor Beta in corneal function, biology and pathology. Curr. Mol. Med 10, 565–578. [PubMed: 20642439]

Tao H, Yang JJ, Shi KH, Li J, 2016. Wnt signaling pathway in cardiac fibrosis: New insights and directions. Metabolism 65, 30–40. [PubMed: 26773927]

Thomas PD, Campbell MJ, Kejariwal A, Mi H, Karlak B, Daverman R, Diemer K, Muruganujan A, Narechania A, 2003. PANTHER: a library of protein families and subfamilies indexed by function. Genome Res 13, 2129–2141. [PubMed: 12952881]

Usui T, Takase M, Kaji Y, Suzuki K, Ishida K, Tsuru T, Miyata K, Kawabata M, Yamashita H, 1998. Extracellular matrix production regulation by TGF-beta in corneal endothelial cells. Invest Ophthalmol Vis Sci 39, 1981–1989. [PubMed: 9761276]

Valiente-Alandi I, Potter SJ, Salvador AM, Schafer AE, Schips T, Carrillo-Salinas F, Gibson AM, Nieman ML, Perkins C, Sargent MA, Huo J, Lorenz JN, DeFalco T, Molkentin JD, Alcaide P, Blaxall BC, 2018. Inhibiting Fibronectin Attenuates Fibrosis and Improves Cardiac Function in a Model of Heart Failure. Circulation 138, 1236–1252. [PubMed: 29653926]

Vincent AL, Niederer RL, Richards A, Karolyi B, Patel DV, McGhee CN, 2009. Phenotypic characterisation and ZEB1 mutational analysis in posterior polymorphous corneal dystrophy in a New Zealand population. Mol Vis 15, 2544–2553. [PubMed: 19997581]

Vlodavsky I, 2001. Preparation of extracellular matrices produced by cultured corneal endothelial and PF-HR9 endodermal cells. Curr Protoc Cell Biol Chapter 10, Unit 10 14.

Weller JM, Zenkel M, Schlotzer-Schrehardt U, Bachmann BO, Tourtas T, Kruse FE, 2014. Extracellular matrix alterations in late-onset Fuchs' corneal dystrophy. Invest Ophthalmol Vis Sci 55, 3700–3708. [PubMed: 24833739]

Wells RG, 2013. Tissue mechanics and fibrosis. Biochim. Biophys. Acta 1832, 884–890. [PubMed: 23434892]

Wilmarth PA, Riviere MA, David LL, 2009. Techniques for accurate protein identification in shotgun proteomic studies of human, mouse, bovine, and chicken lenses. J Ocul Biol Dis Infor 2, 223–234. [PubMed: 20157357]

Wilson SE, Bourne WM, 1988. Fuchs' dystrophy. Cornea 7, 2–18. [PubMed: 3280235]

Wipff PJ, Rifkin DB, Meister JJ, Hinz B, 2007. Myofibroblast contraction activates latent TGF-beta1 from the extracellular matrix. J Cell Biol 179, 1311–1323. [PubMed: 18086923]

Xia D, Zhang S, Nielsen E, Ivarsen AR, Liang C, Li Q, Thomsen K, Hjortdal JO, Dong M, 2016. The Ultrastructures and Mechanical Properties of the Descement's Membrane in Fuchs Endothelial Corneal Dystrophy. Sci. Rep 6, 23096. [PubMed: 26980551]

Yamada KM, Cukierman E, 2007. Modeling tissue morphogenesis and cancer in 3D. Cell 130, 601–610. [PubMed: 17719539]

Yemanyi F, Vranka J, Raghunathan V, 2020a. Generating cell-derived matrices from human trabecular meshwork cell cultures for mechanistic studies. Methods Cell Biol 156, 271–307. [PubMed: 32222223]

Yemanyi F, Vranka J, Raghunathan V, 2020b. Generating cell-derived matrices from human trabecular meshwork cell cultures for mechanistic studies, in: Caballero D, Kundu SC, Reis RL (Eds.), Methods Cell Biol., 1 ed. Academic Press, London, United Kingdom, pp. 271–307.

Zhang C, Bell WR, Sundin OH, De La Cruz Z, Stark WJ, Green WR, Gottsch JD, 2006. Immunohistochemistry and electron microscopy of early-onset fuchs corneal dystrophy in three cases with the same L450W COL8A2 mutation. Trans Am Ophthalmol Soc 104, 85–97. [PubMed: 17471329]

Highlights

- Bovine corneal endothelial cells deposit a matrix while maintaining cellular morphology
- Matrix deposited after TGFβ treatment are softer akin to human FECD
- Cell derived matrices may model cell-matrix interactions for FECD biology

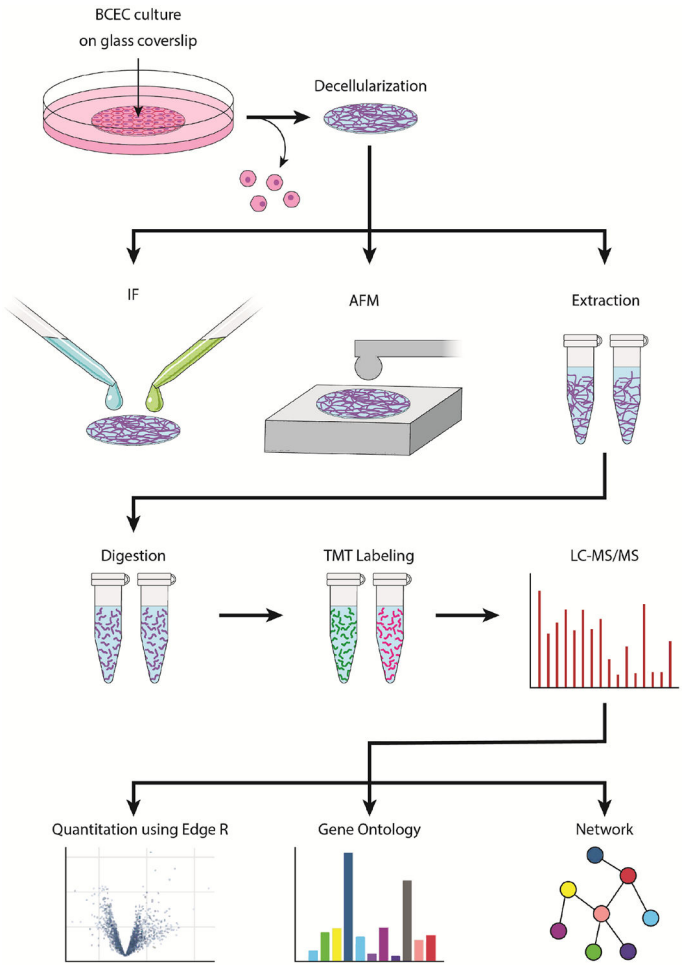

Fig. 1. Schematic flowchart demonstrating the experimental design and analysis steps.

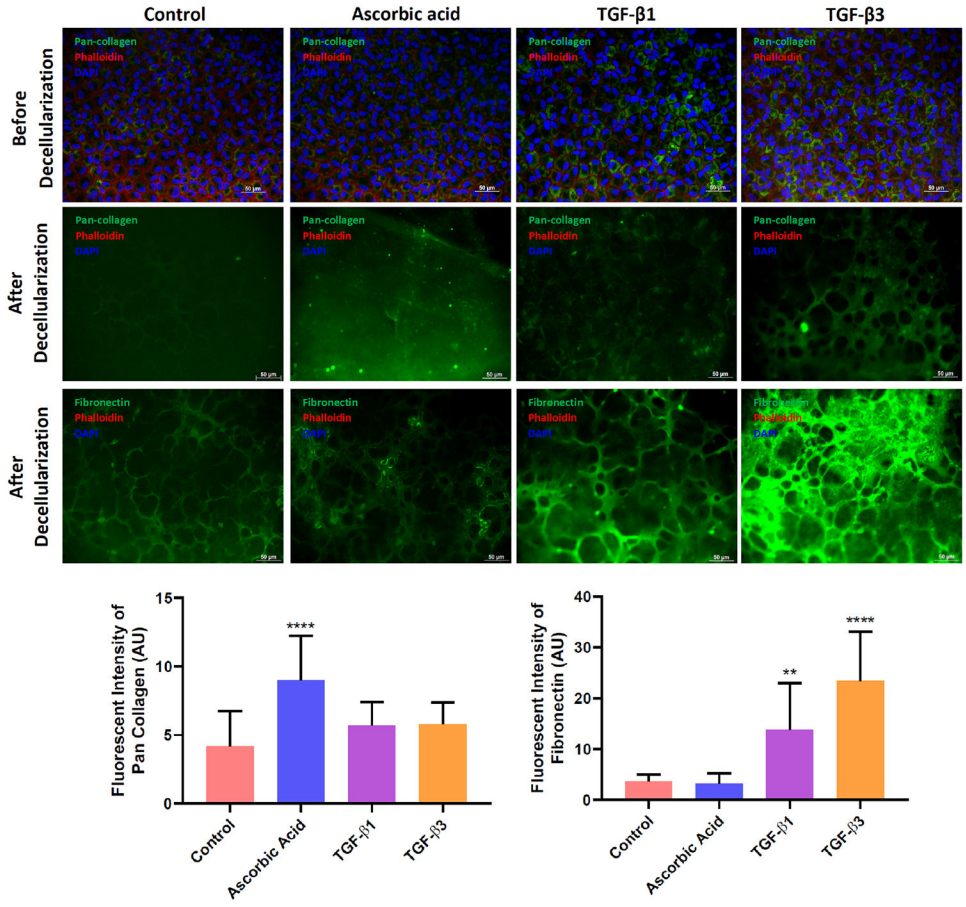

Fig. 2. Structure and expression of collagen and fibronectin is modulated by TGF-β1 and TGFβ3.

Representative images of samples stained with pan-collagen, fibronectin, phalloidin and DAPI prior to decellularization (Top row), and after decellularization stained with pan-collagen (middle row), fibronectin (bottom row), phalloidin and DAPI. Bar graphs illustrate the quantification (relative fluorescent intensity) of pan-collagen and fibronectin amounts in decellularized matrices. Bar graphs are mean ± standard deviation from n = 4 independent experiments. One-way ANOVA was used for statistical analysis followed by Tukey's multiple comparison test. **p<0.01 and ****p<0.0001 compared with control group.

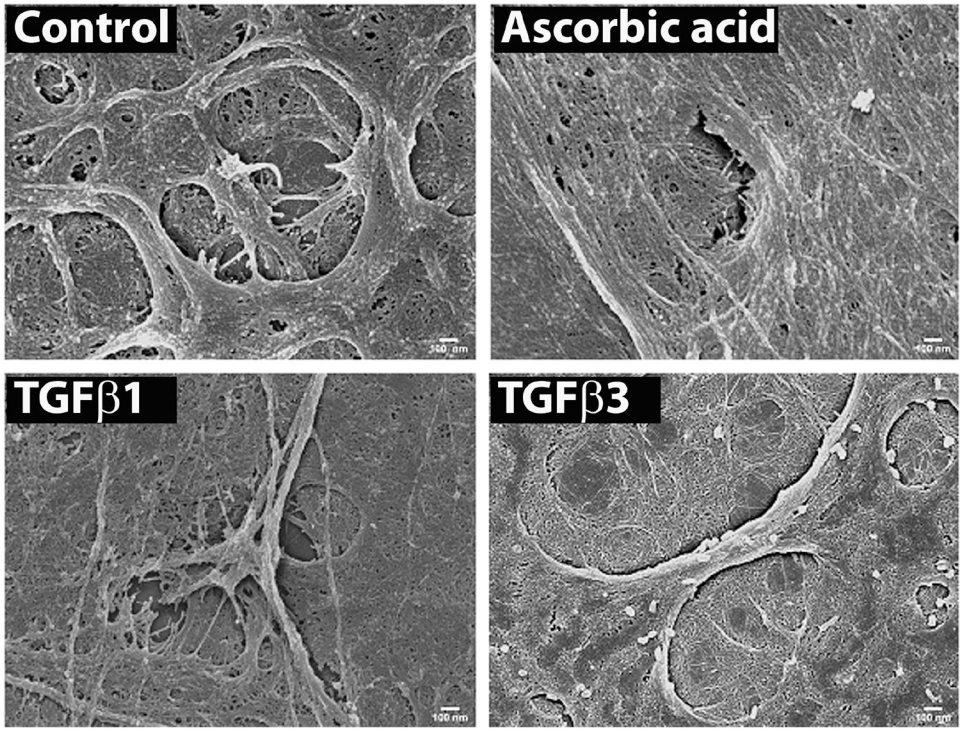

Fig. 3. Scanning Electron Microscope images of the ECM deposited by the BCECs.

Representative images of the ECM derived from the untreated BCECs and those treated with AA, TGF-β1 and TGF-β3. Samples were decellularized, fixed, and coated with gold before imaging.

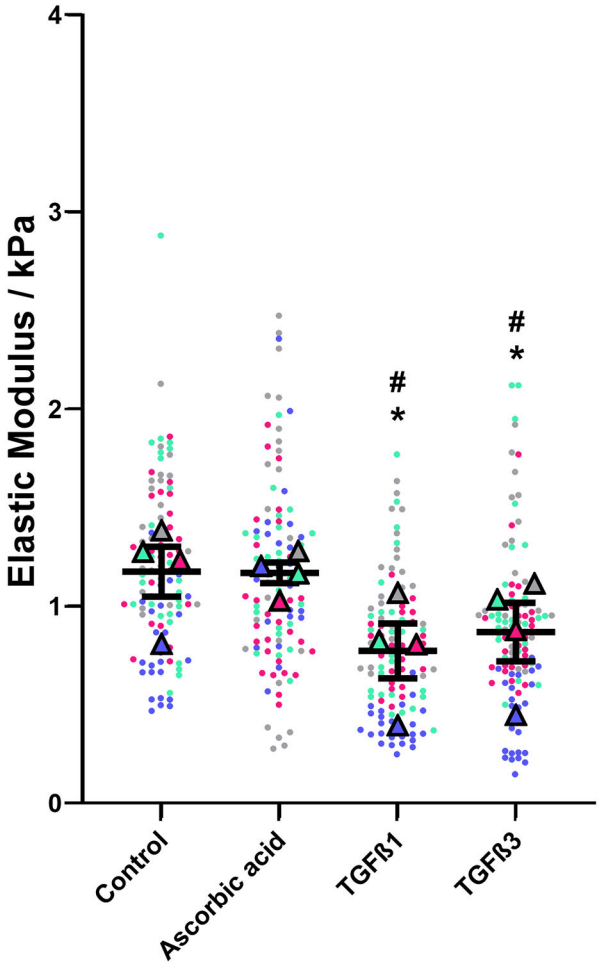

Fig. 4. Elastic modulus of the ECM was significantly lower when BCECs are treated with TGF-β1 and TGF-β3 and AA.

Elastic modulus of the ECM of the BCECs treated with AA, TGF-β1 and TGF-β3 is expressed as a SuperPlot. Individual dots represent individual modulus values from each force curve. Scatter plot (represented by ▲) indicate mean ± SD of moduli values obtained from each of $n = 4$ independent experiments (represented by different colors). One-way ANOVA was used for statistical analysis followed by Tukey's multiple comparison test. * $P < 0.05$ compared with control; # $P < 0.05$ compared to AA treated matrix.

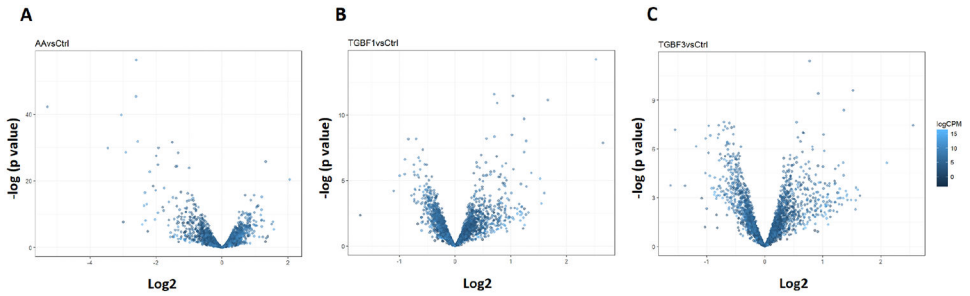

Fig. 5. Differential expression of ECM proteins in each treatment compared to control.

(A-C) Volcano plots exhibiting the abundance differences and differential expression significance of ECM proteins in BCECs treated with (A) AA, (B) TGF-β1 and (C) TGF-β3 compared to control. Each dot is a representative of individual protein. The X-axis indicates the log2 fold change of proteins in a treated sample relative to control sample. $n = 5$ for each treatment.

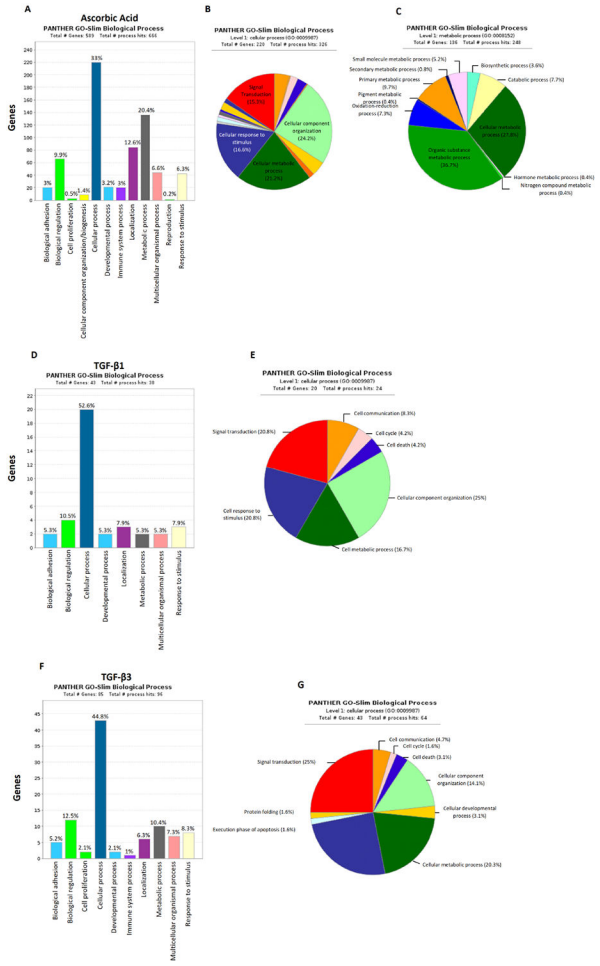

Fig. 6. AA-treated samples showed more biological processes compared to TGF-treated cells.

(A) AA-treated BCECs show various cellular processes. Among biological process annotations, cellular and metabolic processes showed higher enrichment compared to other pathways. (B-C) Further analysis of the cellular and metabolic processes observed in AA-treated samples (D) Biological processes identified in the TGF-β1-treated samples. (E) Breakdown of the cellular processes observed in TGF-β1-treated samples. (F) Biological process identified in the TGF-β3-treated samples. (G) Further analysis of the cellular processes found in TGF-β3-treated cells.

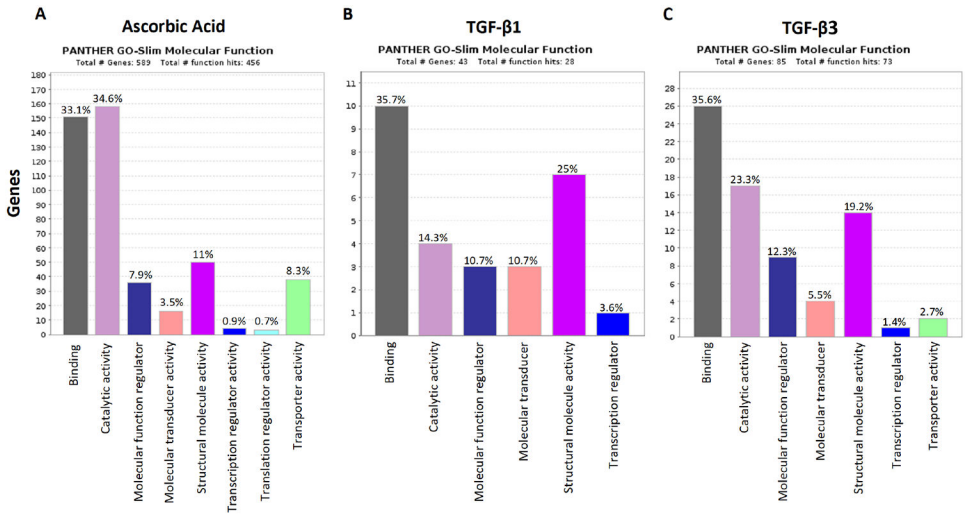

Fig. 7. AA and TGF-β specifically modulate different molecular functions in ECM of the BCECs.
(A) Gene Ontology analysis showed that AA increases catalytic and binding activity in the ECM. (B-C) Binding and structural activity of the ECM increases in response to TGF-β1 and TGF-β3.

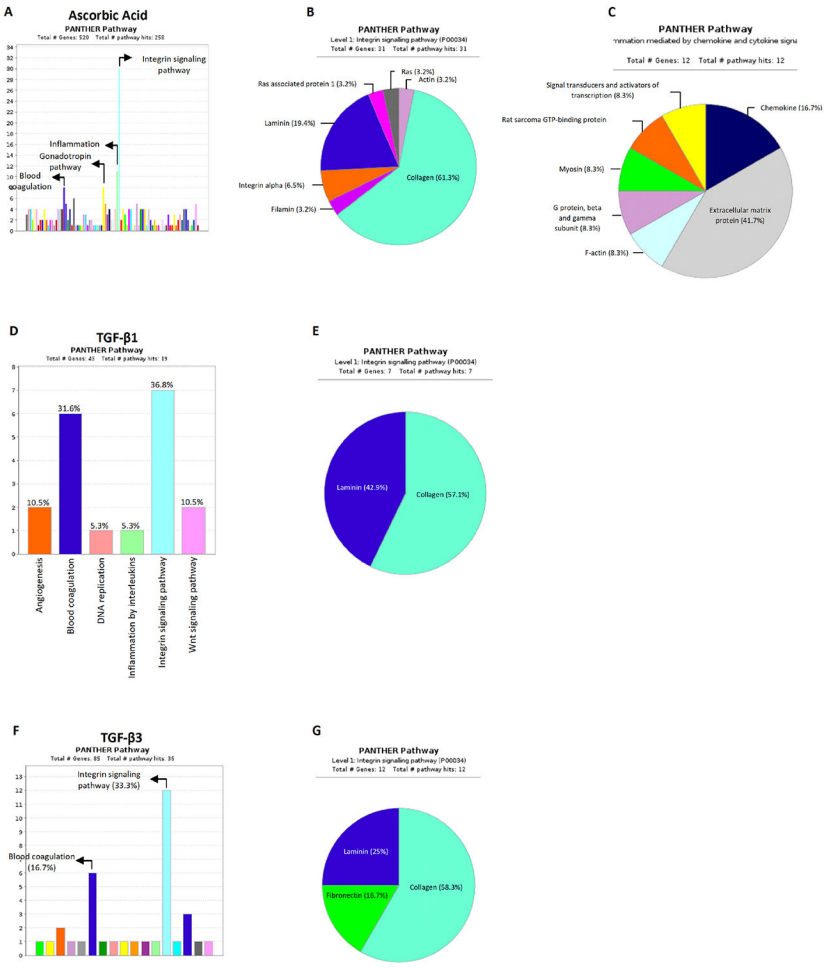

Fig. 8. AA and TGF-β induce various biochemical pathways in the ECM.

(A) AA modulated many biochemical pathways including integrin signaling and inflammation pathway. (B-C) Analysis of the integrin and inflammation pathway showed that AA triggers these pathways directly through differential expression of the ECM components. (D-G) Integrin signaling pathways increases in the presence of TGF-β1 and TGF-β3. Analysis of this pathway for both TGFβ isoforms revealed upregulation of ECM-based proteins in the matrix.

Table 1.

List of genes and their related proteins relevant to oxidative stress identified in response to AA

UniProt ID	Gene	Protein	Log Fold Change	P Value
Q5E947	PRDX1	Peroxiredoxin-1	0.70801	0.00034134
Q2NL01	GPX8	Probable glutathione peroxidase 8	0.584168	0.00312306
A3KLR9	SOD3	Superoxide dismutase [Cu-Zn]	−1.83328	1.92315E-20

Table 2.

List of genes and their related proteins relevant to integrin signaling and ECM remodeling identified in response to TGF-β3

UniProt ID	Gene	Protein	Log Fold Change	P Value
F1MD77	LAMC1	Laminin subunit gamma 1	1.345	0.000001
P98133	FBN1	Fibrillin-1	1.343	0.000001
A0JNB6	LOXL1	Lysyl oxidase homolog 1	1.337	0.000001
P79121	TIMP3	Metalloproteinase inhibitor 3	1.332	0.000001
F1MZU6	COL4A3	Collagen alpha-3(IV) chain	1.284	0.000003
F1N474	COL4A5	Collagen type IV alpha 5 chain	1.28	0.000003
F1N7Q7	COL4A2	Collagen alpha-2(IV) chain	1.225	0.000008
F1MNT4	LAMB1	Laminin subunit beta 1	1.222	0.000009
F1MC13	LAMA5	Laminin subunit alpha 5	1.152	0.000028
F1MJY9	COL4A6	Collagen type IV alpha 6 chain	1.053	0.000127
F1N0C7	NTN1	Netrin 1	1.025	0.000191
F1MJ71	COL4A4	Collagen type IV alpha 4 chain	0.959	0.000482
F1N1Z6	ITIH5	Inter-alpha-trypsin inhibitor heavy chain H5	0.901	0.001041
Q3ZBS7	VTN	Vitronectin	0.8887	0.001218